ISBN: 978-3-95450-262-2 ISSN: 2673-5350 doi: 10.18429/JACoW-IBIC2025-MOPMO02

DESIGN STUDIES OF A RETARDING POTENTIAL ENERGY ANALYSER (RPEA) FOR LOW ENERGY ANTIMATTER EXPERIMENTS

B. S. Rawat*,[1,2], N. Kumar[1,2], S. Chandran[1,2], B. Rienacker[1], C. P. Welsch[1,2]
[1] Department of Physics, University of Liverpool, Liverpool, UK
[2] Cockcroft Institute, Sci-Tech Daresbury, Warrington, UK

Abstract

Retarding Potential Energy Analysers (RPEAs) are widely used diagnostic instruments for measuring the energy distribution of charged particle beams. In this work, we will discuss the conceptual design studies of a RPEA for low energy antimatter beams (antiprotons/positrons). Simulation tools such as CST Studio and G4Beamline were used to study the prototype RPEA and for different geometries to consider effects parameters such as beam properties, collector geometry, the losses occurring due to secondary electrons and annihilations, etc. The proposed diagnostic can offer the potential to measure the energy and current of low energy (1–10 keV) antiproton/positron bunches in experiments such as AE$\bar{g}$IS, with promising energy resolution. In addition, detailed studies are required to assess its viability and improve its accuracy for implementation in a practical experimental setup.

INTRODUCTION

Retarding Potential Energy Analyzers (RPEAs) are beam diagnostic instruments that are used to measure the energy distribution function of an incoming charged particle beam [1]. They typically consist of a series of grids that serve different purposes, such as energy discrimination and suppressing secondary electrons. However, gridless (without meshed grids) RPEAs have also been demonstrated [2,3], where no mesh grid is used for particle energy discrimination. In antimatter detection, annihilation at the collector surface generates secondary particles (photons, pions, neutrons) leading to signal loss. To quantify and minimize these losses, we use G4Beamline simulations [4] to evaluate collector materials behavior and CST Studio [5] to simulate the Discriminator Electrode (D.E.) for particle filtering and determining the Energy Distribution Function (E.D.F).

G4Beamline MODEL

G4Beamline, a Geant4-based toolkit for beamline design and optimization, was used to simulate secondary particles from antiproton/positron interactions with various collector materials. Figure 1 shows the typical RPEA simulation setup. The system includes a main collector and a Discriminator Electrode (D.E.) located near the entrance. Although the collector material is varied across simulations, the D.E. modeled using stainless steel. In the current study, initially a gridless D.E model was used for the G4Beamline simulations to minimize the computational load due to the secondaries formed due to the antiproton / positron interaction, whereas later for the filtering simulation, a meshed D.E was used in the CST simulation. Two cylindrical scoring volumes (labeled side and forward detectors, shown in green) register secondary particles that escape the interaction region, with dimensions shown in Fig. 1. The dimensions are not optimal, but were chosen to ensure efficient scoring of the secondary particles. A 10 keV antiproton beam with 100,000 events was simulated, using typical beam properties from the literature [6], with widths of 0.5 – 2.5 mm depending on the collector geometry. Secondary particles escaping back toward the RPEA entrance were not considered.

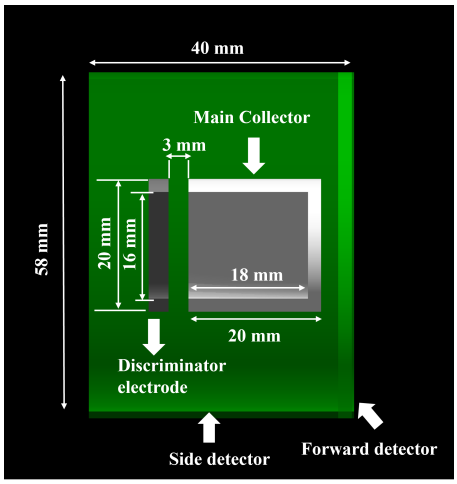

Figure 1: G4Beamline simulation setup of the RPEA with the collector and the Discriminator Electrode (D.E.).

SECONDARY PARTICLE DISTRIBUTIONS

To investigate the effect of secondary particle production on various collector materials, G4Beamline particle tracking simulations were performed for the collector geometry using different materials. An example of the energy distribution of secondary particles formed by the interaction of a 10 keV antiproton beam on a copper collector is shown in Fig. 2. The x-axis corresponds to the particle energy in MeV, and the y-axis represents the number of particles (N). Unlike normal particles, antiprotons annihilate upon interacting with the collector material, producing a variety of secondary particles, including electrons, pions, photons, and others. As shown in Fig. 2, charge loss is mainly due to high energy gamma rays (magenta) and neutrons (cyan). In normal matter beams, secondary electrons are the main issue and are suppressed electrostatically or magnetostatically. For

* bharat26@liverpool.ac.uk

Content from this work may be used under the terms of the CC BY 4.0 licence (© 2025). Any distribution of this work must maintain attribution to the author(s), title of the work, publisher, and DOI.

ISBN: 978-3-95450-262-2 ISSN: 2673-5350 doi: 10.18429/JACoW-IBIC2025-MOPMO02

Content from this work may be used under the terms of the CC BY 4.0 licence (© 2025). Any distribution of this work must maintain attribution to the author(s), title of the work, publisher, and DOI.

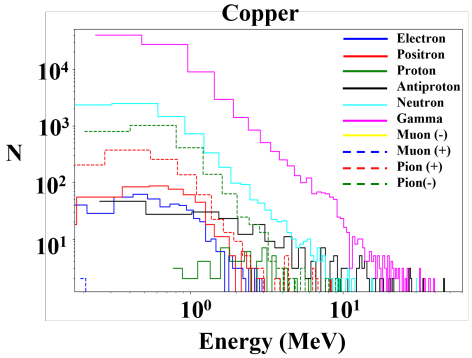

Figure 2: Energy distribution of secondary particles produced by a 10 keV antiproton beam on copper collector.

antimatter beams, high energy pions (dotted red/green)and neutrals dominate the charge loss mechanism, where such suppression methods are ineffective. Figure 3 presents the energy distribution of the secondary particles for carbon as the collector material. It is clear from the plot that because of its low atomic number, the neutron yield of carbon is lower compared to higher Z materials, which helps reduce neutron related charge losses. Thus, a carbon (graphite) collector may be considered a favorable option for this aspect. However, a comprehensive evaluation of losses from muons, gamma rays, and other secondary particles by estimating the total number of particles (area under the curve) is still required and falls beyond the present scope. Similarly, Fig. 4 shows the energy distribution of secondary particles generated from the interaction of a 10 keV positron beam with a carbon collector. The spectrum shows contributions from secondary electrons and the gammas emitted from the collector surface. The variation of the collector's collection angle on the distribution of secondary particles was then investigated. Figure 5 illustrates two of the studied collector geometries; however, simulations were performed for collection angles of 15°, 30°, 45°, and 60°. To ensure that the entire antiproton beam is collected with the smallest possible acceptance angle (15°) in these simulations, the beam width was reduced from 2.5 mm to 0.5 mm. This ensures that no primary particles are cut off. Figures 5 (a) and (b) show the 15°and 45° setups for antiproton interactions with a carbon

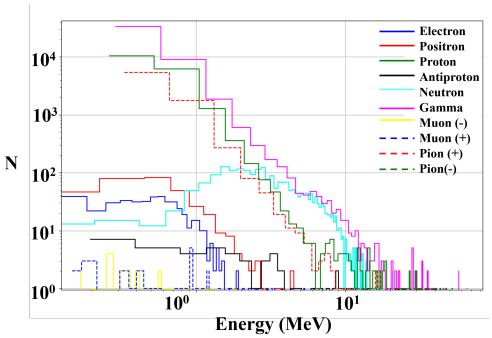

Figure 3: Energy distribution of secondary particles produced by a 10 keV antiproton beam on Carbon collector.

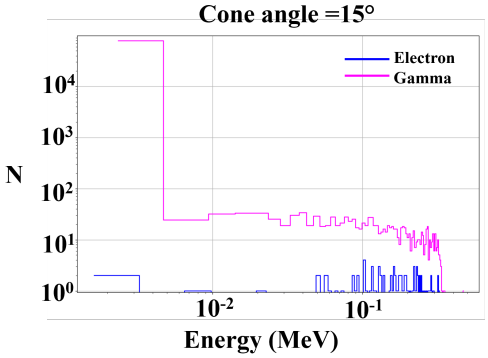

Figure 4: Energy distribution of secondary particles produced by a 10 keV positron beam on Carbon collector.

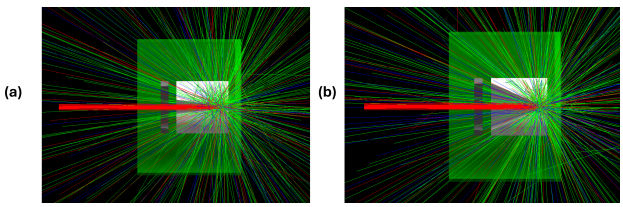

Figure 5: Collector geometries with 15° and 45° collection (cone) angle.

collector. The biggest difference between the two cases is seen in the behavior of the secondary electrons (blue). For the 15° configuration, these electrons are more likely to reinteract with the collector material and have a lower escape probability. In the 45° configuration, the wider collection angle increases the chance of electrons and other secondary particles escaping, adding more error to the measurement.

DISCRIMINATOR ELECTRODE SIMULATIONS

The Discriminator Electrode's (D.E.) energy filtering effect was simulated in CST Studio using the Electrostatic Particle-in-Cell solver. In the simulation a cylindrical geometry collector (Fig. 1) and a meshed DE at the entrance with a wire thickness of 0.2 mm with a pitch spacing of 1 mm in both x and y directions, as illustrated in Fig. 6. Meshed grids enhance local electric fields but cause annihilation losses, unlike gridless designs. Since secondary electron emission is not included in the simulations, the collector's collection angle also has a minimal effect on the output, so we used the geometry shown in Fig. 1, but with a meshed grid for better energy discrimination. The antiproton source was a 3 mm circular area with 374 emission points directed toward the RPEA, 82 mm from the collector's entrance, using a DC PIC emission model with a 0.1 µs rise time and 1 nA beam current. All the components in the simulations were modeled as PECs (Perfect Electrical Conductors). To simulate the effect of the energy discrimination process, a ramp potential varying from 0 to -10 keV was applied to the D.E. in a time period of 100 ms, as indicated by the blue curve in Fig. 7 . This filters the particles according to their energy, and the current is measured at the RPEA collector.

ISBN: 978-3-95450-262-2 ISSN: 2673-5350 doi: 10.18429/JACoW-IBIC2025-MOPMO02

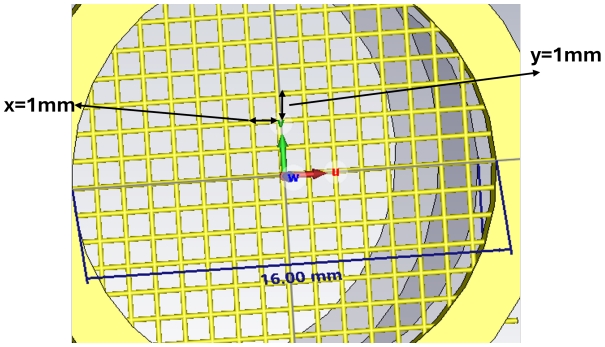

Figure 6: Dimensions of the Discriminator Electrode (D.E.) with Outer Diameter = 20 mm and Inner Diameter ID = 16 mm.

The FC voltage is kept around 10 V, which is suitable in redirecting the secondary electrons and other low energy particles back to the collector surface and minimizing their error contribution. The current measured by the collector is shown in Fig. 7 in the red marker.

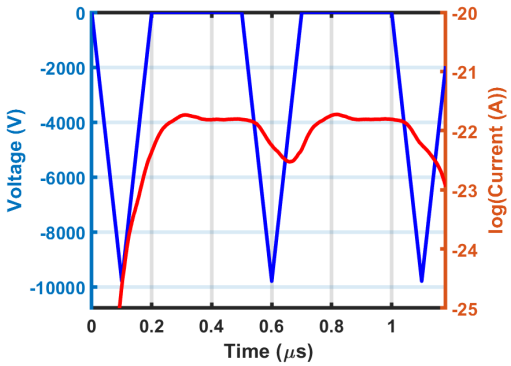

Figure 7: Simulated I-V characteristics of the prototype RPEA. The input ramp signal on the D.E is shown in Blue (0 to -10 keV) and the collector current is shown in red (log scale).

The velocity distribution of the incoming antiproton beam can be expressed by the Maxwell-Boltzmann relationship shown in Eq. (1). Assuming the energy distribution of the incident antiproton to follow the Maxwell- Boltzmann form;

$$F(v) = n\left(\frac{m}{2\pi kT}\right)^{3/2} \exp\left(-\frac{mv^2}{2kT}\right), \qquad (1)$$

where n is the number density, m is the antiproton mass, k is the Boltzmann constant,v is the particle velocity, and T is the effective thermal spread of the beam. In an RPEA, particles with a kinetic energy $E = \frac{1}{2}mv^2$ smaller than qV_r are rejected by the electrostatic potential V_r, where q is the antiproton charge. Eq. (2) can be mathematically derived from Eq. (1).

$$\frac{dI}{dV_r} = -C\frac{4\pi q}{m} v_{\min} F(v_{\min}), \qquad (2)$$

where, $\frac{dI}{dV_r}$ is the derivative of the collector current w.r.t. the ramp voltage, and $v_{\min}$ is the minimum velocity that the particle must overcome to cross the retarding potential barrier, C is the constant that includes acceptance and detection efficiency.

Other considerations (not included in this work) include angular spread requiring integration over all angles, transmission effects of grids / apertures that need calibration, space charge induced barrier shifts in dense beams, and baseline changes from secondary electrons / pion emission that must be suppressed. A moving average filter was applied to smooth out the noisy current signal obtained from the current signal. To obtain the energy distribution function of the antiproton beam, derivative of the current curve with the discriminating voltage is plotted w.r.t. the applied voltage. The typical energy distribution function is shown in Fig. 8. It is clear from the figure that the energy distribution of the incoming antiproton beam is close to 10 keV. This is expected as the initial antiproton beam source was simulated with a kinetic energy of 10 keV with 50 % spread. However, as can be seen from the EDF plot, the generated signal is quite noisy and may require proper mathematical processing to correctly identify the peak.

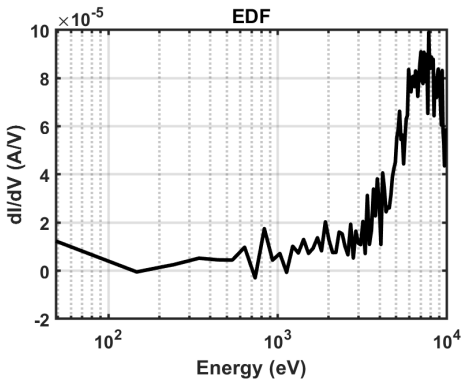

Figure 8: The energy distribution function of the designed RPEA estimated from its I-V characteristics.

CONCLUSION

The feasibility of a prototype RPEA for low energy antimatter beams was investigated through design studies. These preliminary simulations suggest that a carbon (graphite) based collector may serve as an option for estimating the energy distribution of antiproton or positron beams up to tens of keV. Further design refinements and more rigorous simulation studies are required for the realization of such a device. If developed, such an RPEA could potentially provide measurements of both the energy and current of low energy antiproton/positron beams with reasonable accuracy.

ACKNOWLEDGMENTS

This work was supported by EPSRC grant No. EP/XO14851/1, STFC Cockcroft Institute core grant No. ST/V001612/1 and STFC Doctoral Training grant ST/Y509838/1.

Content from this work may be used under the terms of the CC BY 4.0 licence (© 2025). Any distribution of this work must maintain attribution to the author(s), title of the work, publisher, and DOI.

ISBN: 978-3-95450-262-2 ISSN: 2673-5350 doi: 10.18429/JACoW-IBIC2025-MOPMO02

© Content from this work may be used under the terms of the CC BY 4.0 licence (© 2025). Any distribution of this work must maintain attribution to the author(s), title of the work, publisher, and DOI.

REFERENCES

[1] S. T. Lai and C. Miller, "Retarding potential analyzer: Principles, designs, and space applications", *AIP Advances*, vol. 10, no. 9, p. 095324, Sep. 2020. doi:10.1063/5.0014266

[2] N. R. Lobanov, T. Tunningley, and P. Linardakis, "High-resolution grid-less retarding potential analyser and its application for sputter negative ion source", *Nucl. Instrum. Methods Phys. Res. A*, vol. 1050, p. 168169, 2023. doi:10.1016/j.nima.2023.168169

[3] T. W. Shyn, W. E. Sharp, and P. B. Hays, "Gridless retarding potential analyzer for use in very-low-energy charged particle detection", *Rev. Sci. Instrum.*, vol. 47, no. 9, pp. 1005–1015, 1976. doi:10.1063/1.1134828

[4] T. J. Roberts and D. M. Kaplan, "G4beamline simulation program for matter-dominated beamlines", in *Proc. PAC'07*, Albuquerque, NM, USA, pp. 3468–3470, 2007. doi:10.1109/PAC.2007.4440461

[5] CST Studio Suite, https://www.3ds.com/products-services/simulia/products/cst-studio-suite

[6] V. Rodin, "Low-energy beam preparation for the next generation antimatter experiments", Ph.D. dissertation, University of Liverpool, Liverpool, United Kingdom, 2023. https://livrepository.liverpool.ac.uk/3177706/1/201329549_Apr2023.pdf